ANTIOXIDANTS & REDOX SIGNALING
Volume 16, Number 9, 2012

DOI: 10.1089/ars.2010.3849

Mitochondrial Permeability Transition Pore Component Cyclophilin D Distinguishes Nigrostriatal Dopaminergic Death Paradigms in the MPTP Mouse Model of Parkinson's Disease

Bobby Thomas, Rebecca Banerjee, Natalia N. Starkova, Steven F. Zhang, Noel Y. Calingasan, Lichuan Yang, Elizabeth Wille, Beverly J. Lorenzo, Daniel J. Ho, M. Flint Beal, and Anatoly Starkov

Abstract

Aims: Mitochondrial damage due to Ca^{2+} overload-induced opening of permeability transition pores (PTP) is believed to play a role in selective degeneration of nigrostriatal dopaminergic neurons in Parkinson's disease (PD). Genetic ablation of mitochondrial matrix protein cyclophilin D (CYPD) has been shown to increase Ca^{2+} threshold of PTP *in vitro* and to prevent cell death in several *in vivo* disease models. We investigated the role of CYPD in a mouse model of MPTP (1-methyl-4-phenyl-1,2,3,6-tetrahydropyridine)-induced PD. ***Results:*** We demonstrate that *in vitro*, brain mitochondria isolated from CYPD knockout mice were less sensitive to MPP+ (1-methyl-4-phenyl-pyridinium ion)-induced membrane depolarization, and free radical generation compared to wild-type mice. CYPD knockout mitochondria isolated from ventral midbrain of mice treated with MPTP *in vivo* exhibited less damage as judged from respiratory chain Complex I activity, State 3 respiration rate, and respiratory control index than wild-type mice, whereas assessment of apoptotic markers showed no differences between the two genotypes. However, CYPD knockout mice were significantly resistant only to an acute regimen of MPTP neurotoxicity in contrast to the subacute and chronic MPTP paradigms. ***Innovation:*** Inactivation of CYPD is beneficial in preserving mitochondrial functions only in an acute insult model of MPTP-induced dopaminergic neurotoxicity. ***Conclusion:*** Our results suggest that CYPD deficiency distinguishes the modes of dopaminergic neurodegeneration in various regimens of MPTP-neurotoxicity. *Antioxid. Redox Signal.* 16, 855–868.

Introduction

PARKINSON'S DISEASE (PD) is a chronic neurodegenerative movement disorder characterized by progressive degeneration of nigrostriatal dopaminergic neurons. The majority of PD cases are sporadic, with a fraction of them resulting from mutations in known familial PD linked genes (53). A widely used animal model of parkinsonism utilizes the dopaminergic neurotoxin MPTP (1-methyl-4-phenyl-1,2,3,6-tetrahydropyridine) that replicates the selective neuronal loss seen in PD. MPTP causes parkinsonism via its active metabolite 1-methyl-4-phenylpyridinium ion (MPP^+) leading to significant depletion of striatal dopamine and its metabolites, impaired dopamine uptake, ensued by nigral dopaminergic neuronal loss (41). Although the molecular events leading to the loss of dopaminergic neurons in PD remain elusive, compelling evidence suggests that mitochondrial dysfunction could represent a critical triggering event (5).

Mitochondria play a critical role in mediating both apoptotic and necrotic cell death. Accumulation of Ca^{2+} in mi-

Innovation

Ca^{2+} overload-induced opening of the mitochondrial permeability transition pore is believed to play a pathogenic role in the selective loss of midbrain dopaminergic neurons in Parkinson's disease. In this study, we explored the role of mitochondrial permeability transition pore regulatory component cyclophilin D (CYPD) in impacting mitochondrial dysfunctions and nigrostriatal dopaminergic neurodegeneration induced by parkinsonian neurotoxin MPTP (1-methyl-4-phenyl-1,2,3,6-tetrahydropyridine), utilizing CYPD knockout mice. Our studies demonstrate that increasing mitochondrial Ca^{2+} capacity by deactivating CYPD may provide temporary advantage under conditions of acute Ca^{2+} overload. However, elevated Ca^{2+} capacity is not advantageous upon prolonged exposure to mitochondria-damaging toxin, such as MPTP, thereby distinguishing the mode of neurodegeneration as seen in acute, subacute, and chronic intoxication paradigms.

Department of Neurology and Neuroscience, Weill Medical College of Cornell University, New York, New York.

tochondria above a certain level opens a permeability transition pore (PTP) that is described as an abrupt increase in the permeability of inner membrane to solutes with molecular masses of <1500 Da. A transient activation of the PTP is likely to mediate the fast release of Ca^{2+} from the mitochondrion under normal conditions (26, 38). However, overload of mitochondria with Ca^{2+} as a consequence of pathological insult results in inappropriate activation of the PTP, leading to dissipation of the membrane potential, expansion of the matrix, and rupture of the mitochondrial outer membrane (8, 59). Whereas these structural changes render mitochondria bioenergetically dysfunctional and increase the production of reactive oxygen species (1), they also are frequently associated with a concomitant release of pro-apoptotic factors and initiation of apoptotic cell death (5). Thus, blocking PTP could in theory protect cells from both necrotic (*e.g.*, caused by bioenergetics failure) and apoptotic death. The protein composition of PTP remains elusive. However, it is established that the Ca^{2+} threshold of PTP opening is regulated to a certain extent by cyclophilin D (CYPD) (the *Ppif* gene product), which is a peptidyl prolyl isomerase located within the mitochondrial matrix (51). Genetic ablation of CYPD or its inactivation with cyclosporine A has been shown to increase Ca^{2+} threshold of PTP opening *in vitro* and prevent cell death in several *in vivo* disease models (4, 6, 35, 44).

This study was aimed at exploring the potential role of CYPD in nigrostriatal dopaminergic neurodegeneration seen in acute, subacute, and chronic paradigms of MPTP intoxication in mice. Our results suggest that CYPD-regulated mitochondrial PTP is apparently involved in neuronal death observed in acute regimen of MPTP-neurotoxicity, but does not play a significant role in the apoptotic mode of neurodegeneration associated with subacute and/or chronic paradigm of MPTP neurotoxicity.

Results

CYPD ablation attenuates in vitro *Ca^{2+}-induced mitochondrial dysfunction both in the absence and in the presence of MPP^+*

The membrane potential is one of the major factors affecting the Ca^{2+} threshold of PTP opening in mitochondria. It is well established that de-energizing of Ca^{2+}-loaded mitochondria lowers the Ca^{2+} threshold for PTP opening (8). *In vivo*, MPTP is converted to MPP^+ that is accumulated by mitochondria and inhibits the Complex I of the respiratory chain (40, 50), which results in the inability of mitochondria to maintain their membrane potential (13). Therefore, we examined whether *in vitro* MPP^+ accumulation in brain mitochondria would affect their ability to handle Ca^{2+} loading and whether CYPD deficiency is still beneficial under such conditions. Figure 1A demonstrates that as expected, CYPD knockout mitochondria exhibited pronounced resistance to the decrease in steady-state membrane potential upon progressive Ca^{2+} loading (Fig. 1A) and that CYPD knockout mitochondria were able to accumulate significantly higher amounts of Ca^{2+} (Fig. 1B). Next, on the basis of our earlier published studies (13), we selected the amount of MPP^+ that does not decrease the steady state amplitude of the membrane potential in mitochondria. We have verified by HPLC analysis that this amount of MPP^+ is accumulated by both wild-type and CYPD knockout mitochondria to an equal extent (data not presented). Even this small (20 μM) amount of

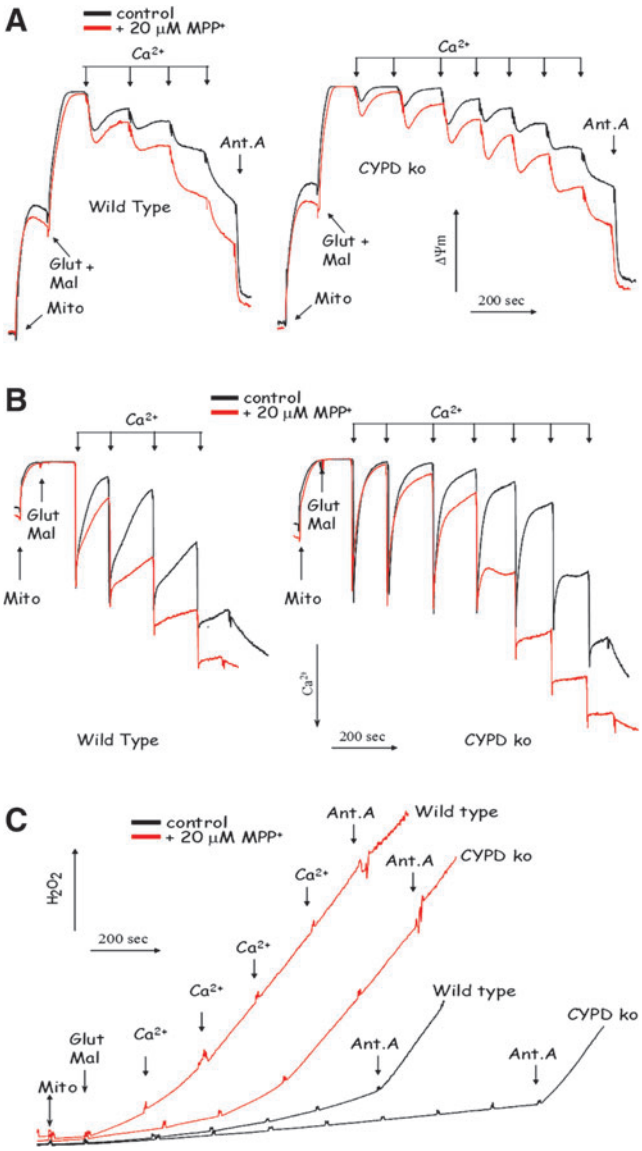

FIG. 1. CYPD ablation attenuates *in vitro* Ca^{2+}-induced mitochondrial dysfunction both in the absence and in the presence of MPP^+. (A) The effect of MPP+ and CYPD deficiency on the membrane potential upon Ca^{2+} loading; **(B)** the effect of MPP+ and CYPD deficiency on Ca^{2+} accumulating capacity of mitochondria; **(C)** the effect of MPP+ and CYPD deficiency on the ROS generation upon Ca^{2+} loading. Abbreviations: Ant.A, addition of 1 μg/ml Antimycin A; Glut Mal, addition of respiratory substrates glutamate and malate; ko MBM, CYPD knockout mouse brain mitochondria; Mito, addition of mitochondria; wt MBM, wild type mouse mitochondria. (To see this illustration in color the reader is referred to the web version of this article at www.liebertonline.com/ars).

MPP^+ exhibited pronounced deleterious effect on both the Ca^{2+}-induced changes in the membrane potential and the Ca^{2+}-accumulating capacity of mitochondria (Figs. 1A and 1B). This deleterious effect of MPP^+ was apparent in both wild type and CYPD knockout mitochondria; however, even in the presence of MPP^+, CYPD knockout mitochondria were able to better maintain their membrane potential and exhibited higher Ca^{2+} capacity than wild-type mitochondria (Figs. 1A and Fig 1B). Thus, although MPP^+ accumulation does augment

Ca^{2+}-induced damage in wild-type and CYPD knockout mitochondria, the latter are still more resistant to MPP^+.

Another pathologically important aspect of mitochondrial Ca^{2+} overload is an increase in reactive oxygen species (ROS) production. Recent literature indicates that PTP opening can strongly stimulate mitochondrial ROS production by disrupting electron flow in the respiratory chain and due to loss of antioxidant compounds such as glutathione and NADPH from the mitochondrial matrix (reviewed in (1)). Earlier data also suggest that MPP^+ accumulation per se can trigger elevated ROS production by mitochondria (2, 29). Therefore, we examined whether CYPD deficiency confers a protection against elevated ROS production in Ca^{2+}-loaded mitochondria. Figure 1C shows that CYPD knockout mitochondria exhibit a higher Ca^{2+} threshold to ROS production both in the absence and in the presence of MPP^+ as compared to wild-type mitochondria. Thus, our data with isolated mitochondria demonstrate that CYPD ablation attenuates the damage to mitochondria induced by Ca^{2+} overload as manifested by higher membrane potential, higher Ca^{2+} accumulating capacity, and lowered ROS production.

CYPD ablation preserves MPTP-induced mitochondrial dysfunctions in ventral midbrain

Next, we examined whether CYPD ablation confers a protection to mitochondrial functions upon *in vivo* treatment with MPTP. Figure 2A shows that ventral midbrain mitochondria (that constitutes less than 5% of substantia nigra pars compacta dopaminergic neurons) isolated from brains of CYPD knockout mice acutely treated with MPTP (see "Methods") exhibited significantly higher activity of respiratory chain Complex I, higher rate of phosphorylating respiration (Fig. 2A, "State 3"), and better respiratory control index (RCI, Fig. 2A), which is an index of structural damage to inner mitochondrial membrane, as compared with MPTP-treated wild-type mice. However, the efficiency of oxidative phosphorylation as represented by the ADP:O ratio was similarly suppressed by about 12% in both wild-type and CYPD knockout mice (Fig. 2A). There were also no differences in several key respiratory chain proteins, ATPase, MnSOD, or cytochrome c content between CYPD knockout and wild-type mitochondria (Figs. 2B and 2C). In line with the data on the membrane potential and oxygen consumption, this indicates the absence of significant difference in bioenergetics capacity or the MPP+-caused structural damage (*e.g.*, rupture of the outer membrane) between wild-type and CYPD knockout mitochondria. We have also checked several pro-apoptotic

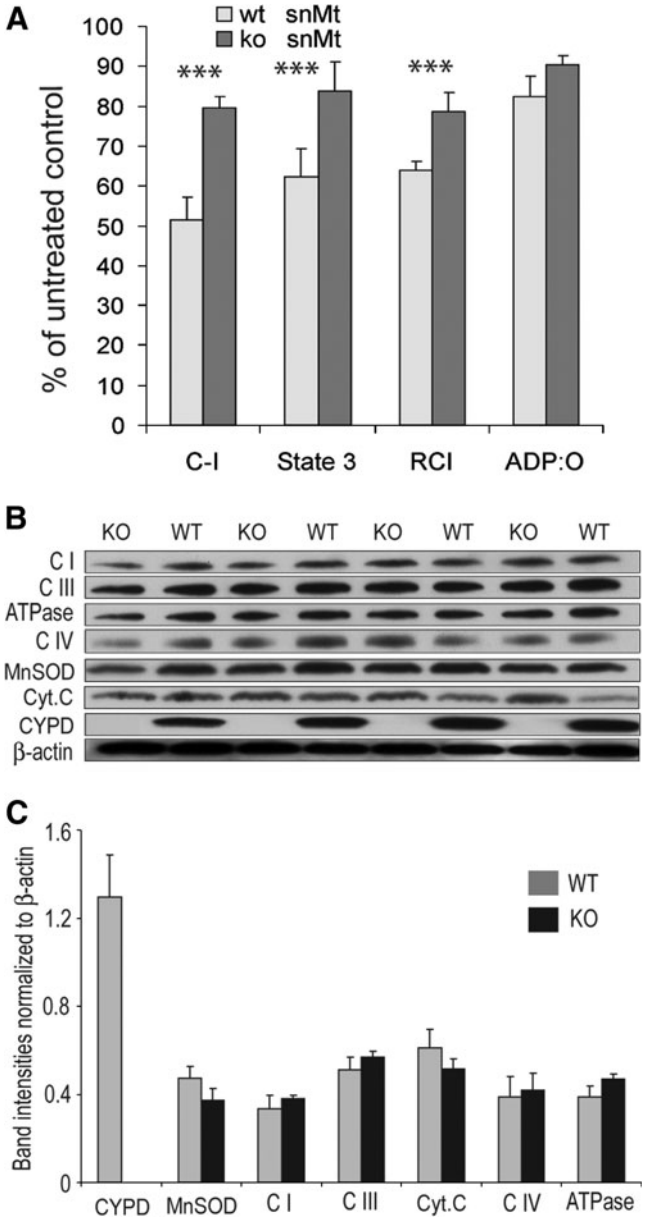

FIG. 2. CYPD ablation preserves mitochondrial functions in ventral midbrain in MPTP treated mice. (A) Activity of respiratory chain Complex I, the rate of phosphorylating respiration ("State 3"), respiratory control index ("RCI"), and ADP:O ratio were measured in mitochondrial isolated from ventral midbrain comprising of SNpc after 4 h of single MPTP (20 mg/kg) injection. Data are presented in percentage from the corresponding wild-type and CYPD-/- saline-treated controls. Data represent Mean ± SEM, * $p < 0.05$ as compared to wild type; $n = 5$ mice per group. Complex I activity (nmol NADH/min/mg mitochondria) was 397.2 ± 39.1 and 482.8 ± 10.3 (MPTP-treated wild-type and CYPD knockout, respectively), 843.3 ± 41.2 and 626.8 ± 45.9 (saline-treated wild-type and CYPD knockout, respectively). State 3 respiration rate (nmol O2/min/mg mitochondria) was 75.2 ± 8.4 and 91.7 ± 8.2 (MPTP-treated wild-type and CYPD knockout, respectively), 120.4 ± 10.6 and 109.6 ± 13.2 (saline-treated wild-type and CYPD knockout, respectively). RCI was 2.8 ± 0.1 and 4.0 ± 0.2 (MPTP-treated wild-type and CYPD knockout, respectively), 4.4 ± 0.2 and 5.0 ± 0.3 (saline-treated wild-type and CYPD knockout, respectively). ADP:O ratio was 2.94 ± 0.18 and 3.2 ± 0.08 (MPTP-treated wild-type and CYPD knockout, respectively), 3.57 ± 0.15 and 3.54 ± 0.29 (saline-treated wild-type and CYPD knockout, respectively). **(B)** ventral midbrain mitochondrial preparations from MPTP-treated wild-type (WT) and CYPD knockout (KO) mice were immunoblotted for the levels of membrane-located respiratory chain proteins Complex I NDUFB8 subunit ("CI"), Complex III Core 2 subunit UQCR2/QCR2 ("CIII") and Complex IV MT-CO1 subunit ("CIV"), ATPase ATP5A1 subunit ("ATPase"), intermembrane space-located cytochrome C, and matrix proteins MnSOD and CYPD. **(C)** Data presented on **(B)** were quantified using ImageJ software and normalized by β-actin. Data presented as mean ± SEM, $n = 4$ mice per group.

markers such as Bim, Bad, and Bax and anti-apoptotic marker Bcl-2 in mitochondria isolated from ventral midbrain of MPTP-treated wild-type and CYPD knockout mice. Immunoblot analysis found similar levels of Bax and Bcl-2 in MPTP-treated wild-type and CYPD knockout mice, whereas we were unable to detect Bim and Bad in our mitochondrial preparations (data not shown). Overall, these data indicate that a) CYPD knockout mitochondria are not different in their bioenergetics capacity/respiratory chain composition from wild-type mitochondria, and b) CYPD ablation protects mitochondrial bioenergetics in this acute MPTP treatment paradigm.

CYPD knockout mice are resistant to acute MPTP neurotoxicity

To investigate the role of CYPD in mediating MPTP-induced nigrostriatal dopaminergic neurotoxicity, age-matched wild-type CYPD knockout littermate mice received MPTP (20 mg MPTP/kg X4, every 2 hours) or saline. The extent of MPTP-induced loss of tyrosine hydroxylase positive dopaminergic neurons in substantia nigra either at 1 week or 3 weeks after MPTP revealed comparable levels of cell loss in wild-type mice (data not shown). One week following MPTP administration, immunohistochemical analysis for tyrosine hydroxylase positive dopaminergic neurons in substantia nigra and striatum demonstrated a marked reduction in TH-immunopositive neurons in substantia nigra (Fig. 3A) and density of TH-positive fibers in striatum (Fig 3B) when compared to saline controls. CYPD knockout mice showed marked reduction in MPTP-induced loss of tyrosine hydroxylase positive dopaminergic neurons in substantia nigra (Fig. 3A) and TH-positive fibers in striatum (Fig. 3B) when compared to MPTP-treated wild-type mice. Unbiased stereologic counts of total (Nissl-positive) and TH-immunopositive neurons in substantia nigra pars compacta (SNpc) show a statistically significant loss of neurons in MPTP-treated wild-type mice compared to saline controls. However, CYPD knockout mice showed significant attenuation of MPTP-induced loss of total (Nissl-positive) and TH-immunopositive neurons compared to MPTP-treated wild-type mice (Fig. 3C). Consistent with the loss of striatal TH-positive fibers (Fig. 3B), HPLC-electrochemical analysis reveals a profound reduction in striatal dopamine (Fig. 3D) and its metabolites [DOPAC and HVA (Fig. 3E)] in this paradigm of MPTP treatment, in wild-type mice compared to saline-injected controls. However, CYPD knockout mice showed significant rescue of MPTP-induced loss of striatal dopamine (Fig. 3D) and its metabolites [DOPAC and HVA (Fig. 3E)].

CYPD knockout mice are not resistant to subacute MPTP neurotoxicity

It is now well established that the paradigm of MPTP delivery in mice have an effect upon the mode of dopaminergic neuronal death (16, 39). The acute intoxication paradigm of MPTP is known to cause dopaminergic neurodegeneration primarily due to necrosis, whereas the subacute MPTP paradigm may cause apoptotic mechanisms of neuronal death (27, 52). In order to test if neuroprotective effects observed in CYPD knockout mice following acute paradigm of MPTP neurotoxicity also extends to the subacute MPTP paradigm and mediates dopaminergic neurodegeneration by apoptosis, we treated wild-type and CYPD knockout mice with subacute MPTP (30 mg MPTP/kg once daily for 5 days) paradigm.

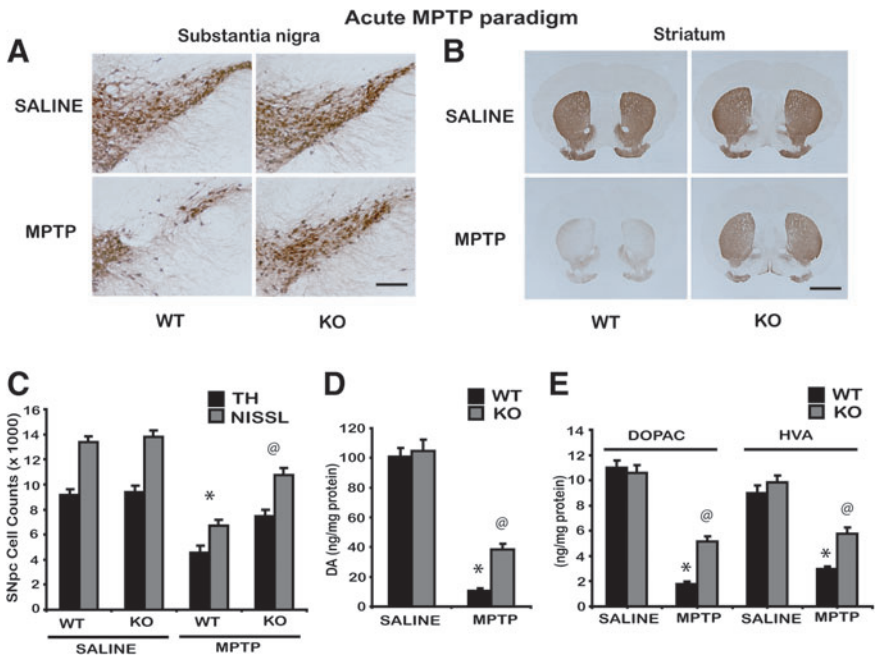

FIG. 3. CYPD knockout mice are resistant to acute paradigm of MPTP neurotoxicity. Male wild-type (WT) and CYPD knockout (KO) littermate mice were intraperitoneally injected with acute MPTP (20 mg/kg free base, every 2 h four times a day). Control animals received saline in the same frequency and volume as MPTP. **(A)** TH-immunostaining of SNpc 7 days following acute MPTP in wild type (WT), CYPD knockout (KO) mice, representative image from $n = 5$ mice in each group, Scale bar, 200 μm. **(B)** TH-immunostaining of striatum 7 days following acute MPTP treatment in wild type (WT), CYPD knockout (KO) mice, representative data from $n = 5$ mice in each group, Scale bar, 200 μm. **(C)** Stereologic cell counts of total and TH-immunopositive neurons of SNpc in wild-type and CYPD knockout mice following MPTP. Data represent mean ± S.E.M. $^{*}p < 0.001$, compared to saline controls and $^{@}p < 0.05$ in comparison to MPTP-treated wild-type using two-way ANOVA followed by Student–Newman–Keuls test, $n = 8$ mice per group. **(D)** Striatal levels of dopamine (DA) measured by HPLC-electrochemistry in wild-type and CYPD knockout mice following MPTP. **(E)** Striatal levels of DOPAC and HVA measured by HPLC-electrochemistry in wild-type and CYPD knockout mice following MPTP. Data represent mean ± S.E.M. $^{*}p < 0.05$, compared to saline controls and $^{@}p < 0.05$ in comparison to MPTP-treated wild-type using two-way ANOVA followed by Student–Newman–Keuls test, $n = 8$–10 mice per group. Values represent as ng per mg protein. (To see this illustration in color the reader is referred to the web version of this article at www.liebertonline.com/ars).

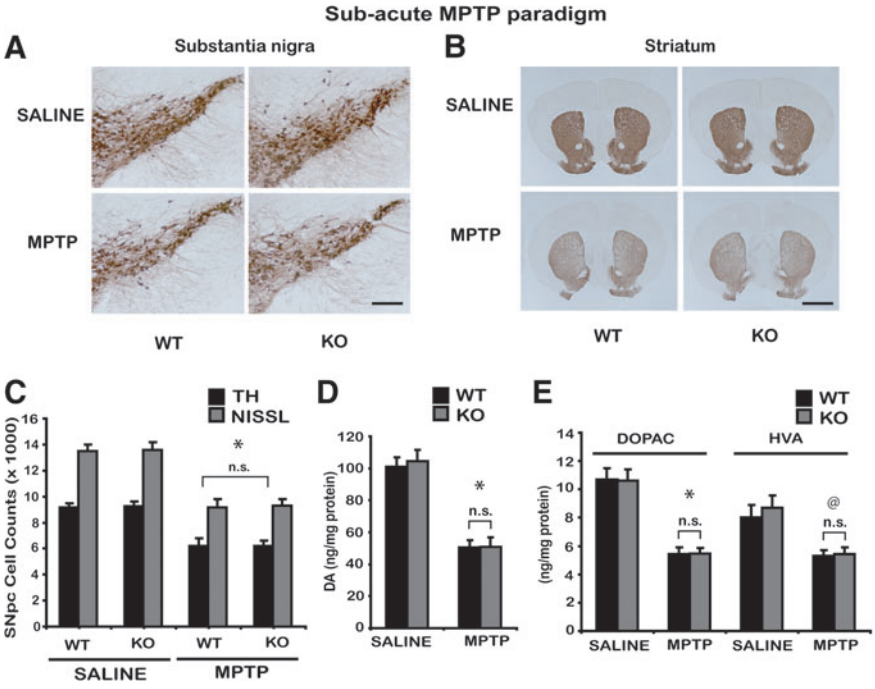

FIG. 4. CYPD knockout mice are not resistant to subacute paradigm of MPTP neurotoxicity. Male wild-type (WT) and CYPD knockout (KO) littermate mice were intraperitoneally injected with subacute MPTP (30 mg/kg free base, once a day for 5 days). Control animals received saline in the same frequency and volume as MPTP. **(A)** TH-immunostaining of SNpc 21 days following last MPTP in wild type (WT), CYPD knockout (KO) mice, representative image from $n=5$ mice in each group, Scale bar, 200 μm. **(B)** TH-immunostaining of striatum 21 days following last MPTP treatment in wild-type (WT), CYPD knockout (KO) mice, representative data from $n=5$ mice in each group, Scale bar, 200 μm. **(C)** Stereologic cell counts of total and TH-immunopositive neurons of SNpc in wild-type and CYPD knockout mice following MPTP. Data represent mean ± S.E.M., $^{*}p<0.001$, compared to saline controls using two-way ANOVA followed by Student–Newman–Keuls test, $n=8$ mice per group. **(D)** Striatal levels of dopamine (DA) measured by HPLC-electrochemistry in wild-type and CYPD knockout mice following MPTP. **(E)** Striatal levels of DOPAC and HVA measured by HPLC-electrochemistry in wild-type and CYPD knockout mice following MPTP. Data represent mean ± S.E.M. $^{@}p<0.05$, compared to saline controls using two-way ANOVA followed by Student–Newman–Keuls test, $n=8$–10 mice per group. Values represent as ng per mg protein. (To see this illustration in color the reader is referred to the web version of this article at www.liebertonline.com/ars).

Three weeks following the last MPTP administration, immunohistochemical analysis for tyrosine hydroxylase positive dopaminergic neurons in substantia nigra and striatum demonstrated a marked reduction in TH-immunopositive neurons in substantia nigra (Fig. 4A) and density of TH immunostaining in striatum (Fig. 4B) compared to saline controls. No significant differences were observed between wild-type and CYPD knockout mice after MPTP. Unbiased stereologic counts of total (Nissl-positive) and TH-immunopositive neurons in SNpc show a statistically significant loss of neurons in wild-type mice compared to saline control. However, CYPD knockout mice failed to demonstrate an attenuation of MPTP-induced loss of total (Nissl-positive) and TH-immunopositive neurons compared to MPTP-treated wild-type mice (Fig. 4C). Consistent with the loss of striatal TH-positive fibers (Fig. 4B), HPLC-electrochemical analysis reveals a profound reduction in striatal dopamine (Fig. 4D) and its metabolites [DOPAC and HVA (Fig. 4E)] in this paradigm of MPTP treatment in wild-type mice compared to saline controls. However, CYPD knockout mice failed to show a rescue against MPTP-induced loss of striatal dopamine (Fig. 4D) and its metabolites [DOPAC and HVA (Fig. 4E)].

CYPD knockout mice are not resistant to chronic MPTP neurotoxicity

Chronic continuous infusion of MPTP employing a subcutaneous implantation of Alzet mini osmotic pumps in mice causes severe nigrostriatal dopaminergic toxicity, accompanied by accumulation of alpha-synuclein in TH-positive neurons of substantia nigra (14, 23, 54). Accordingly, mini osmotic pumps that delivered either saline or 30 mg MPTP/kg/day for 28 days were subcutaneously implanted in wild-type and CYPD knockout mice. After termination of chronic continuous MPTP treatment, TH staining of mesencephalic and striatal brain sections performed the next day showed significant loss of SNpc dopaminergic neurons, compared to saline-treated control animals (Figs. 5A and 5B). No significant differences were observed between wild-type and CYPD knockout mice after MPTP. Unbiased stereologic counts of total (Nissl-positive) and TH-immunopositive neurons in SNpc show a statistically significant loss of neurons in wild-type mice compared to saline control. However, CYPD knockout mice failed to demonstrate an attenuation of MPTP-induced loss of total (Nissl-positive) and TH-immunopositive neurons compared to MPTP-treated wild-type mice (Fig. 5C). Consistent with the loss of striatal TH-positive fibers (Fig. 5B), HPLC-electrochemical analysis revealed a profound reduction in striatal dopamine (Fig. 5D) and its metabolites [DOPAC and HVA (Fig. 5E)] in this paradigm of MPTP treatment, in wild-type mice compared to saline controls. However, MPTP-induced loss of striatal dopamine (Fig. 5D) and its metabolites [DOPAC and HVA (Fig. 5E)] was not attenuated in CYPD knockout mice.

CYPD ablation does not interfere with MPTP metabolism

To determine whether the neuroprotective effect observed in the acute paradigm of MPTP neurotoxicity in CYPD knockout mice is due to insufficient conversion of MPTP to its toxic metabolite MPP^+, we measured striatal levels of MPP^+ in wild-type and CYPD knockout mice. Striatal levels of MPP^+ were measured by HPLC-fluorimetry in 8-week-old CYPD knockout and age-matched wild-type mice at 90, 120, and 360 min after a single injection of MPTP (20 mg/kg free

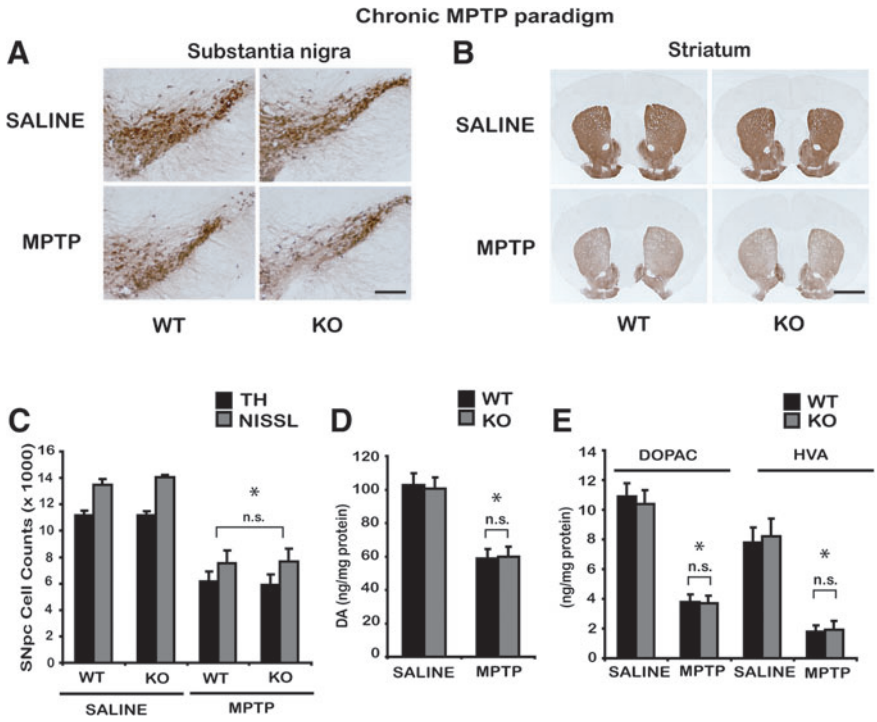

FIG. 5. CYPD knockout mice are not resistant to chronic paradigm of MPTP neurotoxicity. Male wild-type (WT) and CYPD knockout (KO) littermate mice were administered with chronic MPTP (30 mg/kg/day for 28 days). Control animals received saline in the same frequency and volume as MPTP. **(A)** TH-immunostaining of SNpc one day after chronic 28 day MPTP in wild-type (WT), CYPD knockout (KO) mice, representative image from $n=5$ mice in each group, Scale bar, 200 μm. **(B)** TH-immunostaining of striatum following chronic MPTP treatment in wild type (WT), CYPD knockout (KO) mice, representative data from $n=5$ mice in each group, Scale bar, 200 μm. **(C)** Stereologic cell counts of total and TH-immunopositive neurons of SNpc in wild-type and CYPD knockout mice following chronic MPTP. Data represent mean ± S.E.M., $^*p<0.001$, compared to saline controls using two-way ANOVA followed by Student–Newman–Keuls test, n = 8 mice per group. **(D)** Striatal levels of dopamine (DA) measured by HPLC-electrochemistry in wild-type and CYPD knockout mice following MPTP. **(E)** Striatal levels of DOPAC and HVA measured by HPLC-electrochemistry in wild type and CYPD knockout mice following MPTP. Data represent mean ± S.E.M., $^*p<0.001$, compared to saline controls using two-way ANOVA followed by Student–Newman–Keuls test, $n=8$–10 mice per group. Values represent as ng per mg protein. (To see this illustration in color the reader is referred to the web version of this article at www.liebertonline.com/ars).

base). Additionally, striatal MPP^+ levels were also measured following the chronic paradigm of MPTP neurotoxicity in wild-type and CYPD knockout mice the next day after a 28-day infusion of MPTP (30 mg/kg/day). MPP^+ levels in CYPD knockout mice either due to a single injection or chronic infusion of MPTP were not significantly different compared to those in wild-type mice (Table 1), suggesting that lack of CYPD does not impair the conversion of MPTP to MPP^+.

Resistance to acute paradigm of MPTP neurotoxicity in CYPD knockout mice is not by interfering MPTP-induced microglial and astrocytic activation

The degeneration of nigrostriatal dopaminergic neurons in the acute paradigm of MPTP neurotoxicity is marked by robust inflammatory reaction with activation of astrocytes and microglia within the nigrostriatal pathway. It was suggested that blockade of MPTP-induced glial activation could render a neuroprotective effect on nigrostriatal dopaminergic neurons (55). Consequently, it may be that the attenuation of nigrostriatal dopaminergic neurodegeneration following acute paradigm of MPTP-neurotoxicicity observed in CYPD knockout mice could reflect differences due to MPTP-induced activation status of microglia and astrocytes. To investigate this possibility, we assessed MPTP-induced glial response by examining the expression of CD11b, a specific marker for microglia, and GFAP, a marker for astrocytes. As shown in Figure 6A,following acute MPTP injection (20 mg/kg for four injections), GFAP immunoreactivity in substantia nigra of wild-type and CYPD knockout mice was similar compared to saline-injected mice. MPTP administration resulted in a marked increase in reactive astrogliosis by 36 hours after the last MPTP administration both in wild-type and CYPD knockout mice, whereas in saline-treated animals only a few faintly immunoreactive resting astrocytes were observed in substantia nigra (data not shown). Consistent with the qualitative increase in GFAP immunoreactivity, the total counts of GFAP immunoreactive astrocyte were significantly higher in substantia nigra of MPTP-treated wild-type and CYPD knockout mice when compared to saline controls. However,

Table 1. Striatal MPP^+ Levels Following Acute and Chronic MPTP Paradigms in Wild-Type and Cyclophilin D Knockout Mice

Single MPTP administration					*Chronic MPTP paradigm*
	90 min	120 min	180 min	360 min	29^{th} day
WT	7.66 ± 0.07	8.2 ± 0.07	7.8 ± 0.1	0.9 ± 0.08	8.2 ± 0.07
KO	7.61 ± 0.09	8.3 ± 0.09	7.9 ± 0.12	0.8 ± 0.08	8.1 ± 0.09

Striatal MPP + levels in wild-type and cyclophilin D knockout mice at 90, 120, 180, and 360 min after single MPTP-injection administered at 20 mg/kg and on 29^{th} day following the beginning of chronic 28 day MPTP (30 mg/kg/day) infusion. Data represent mean ± SEM for 5–7 mice per group at various time points following single and chronic administration. Values represent as ng per mg weight of the tissue.

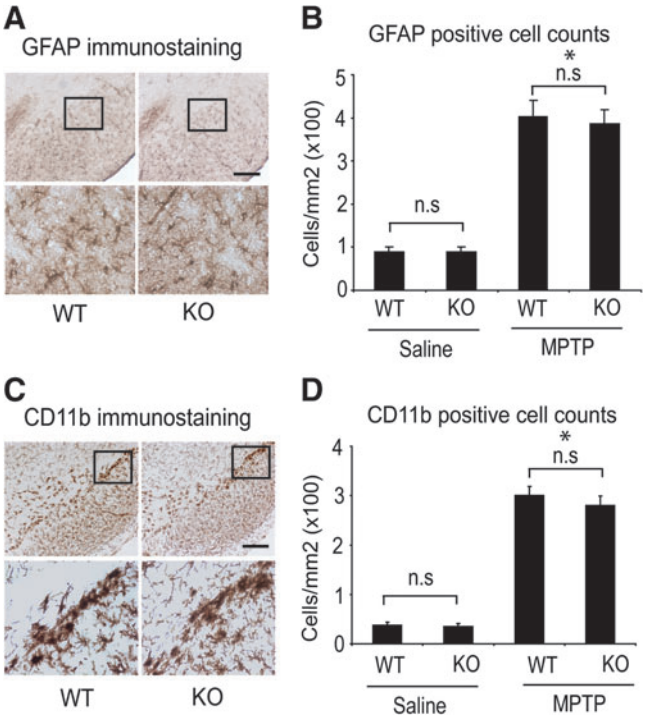

FIG. 6. Resistance to acute MPTP neurotoxicity in CYPD knockout mice is not due to blockade of astrocytic and microglial activation. **(A)** Astrogliosis demonstrated by glial fibrillary acidic protein (GFAP) immunostaining in SNpc of WT and KO mice 2 days after last MPTP treatment following the acute paradigm, representative image from 5 mice in each group. **(B)** GFAP positive reactive astrocytic cell counts in wild-type and CYPD knockout SNpc after 36 hours of last injection of MPTP following acute toxicity paradigm. Data represent mean ± S.E.M., $*p < 0.05$, statistical significance versus saline controls using ANOVA followed by Student–Newman–Keuls test, $n = 5$ mice per group, n.s not significant. **(C)** Microglial activation demonstrated by CD11b (Integrin alpha-M beta-2) immunostaining in SNpc of WT and KO mice 2 days after last MPTP treatment following the acute paradigm, representative image from $n = 5$ mice in each group. **(D)** CD11b positive cell counts in wild-type and CYPD knockout SNpc after 36 hours of last injection of MPTP following acute toxicity paradigm. Data represent mean ± S.E.M., $*p < 0.05$, statistical significance versus saline controls using ANOVA followed by Student–Newman–Keuls test, $n = 5$ mice per group, n.s not significant, Scale bar, 200 μm. (To see this illustration in color the reader is referred to the web version of this article at www.liebertonline.com/ars).

no significant differences were found between wild-type and CYPD knockout mice (Fig. 6B). Similarly, examination of CD11b immunoreactive microglia 36 hours after the last administration of MPTP (20 mg/kg for four injections) showed robust activation of microglia with amoeboid-like morphology in wild-type and CYPD knockout mice (Fig. 6C) in comparison to saline treated mice where microglia were mostly in resting stage (data not shown). Morphometric evaluation of activated CD11b positive microglia in MPTP-treated mice showed a statistically significant increase in activated microglia both in wild-type and CYPD knockout mice compared to saline-treated controls, where as no differences was found between wild- type and CYPD knockout mice following MPTP administration (Fig. 6D). Taken together, these data suggest that CYPD ablation in mice does not alter the activation status of microglia and astrocytes following MPTP administration and indicate that resistance to acute MPTP neurotoxicity in CYPD knockout mice is not due to blockade of microglial and astrocytic activation.

CYPD ablation does not impact MPTP-induced apoptotic death of TH-positive neurons and alpha-synuclein accumulation in substantia nigra

The nigrostriatal dopaminergic neurodegeneration seen in the subacute paradigm of MPTP neurotoxicity in mice is characterized by apoptotic cell death (27, 52). To determine if failure of CYPD knockout mice to block dopaminergic neurodegeneration seen in the subacute paradigm of MPTP neurotoxicity is due to its inability to block apoptotic cell death, we investigated the presence of apoptotic markers in substantia nigra. As shown in Figure 7A, following subacute MPTP injection (30 mg/kg once daily for 5 days) tyrosine hydroxylase and thionin-positive apoptotic neurons were observed in SNpc of wild-type and CYPD knockout mice compared to saline-injected mice. Two days after the last administration of MPTP, there was a significant proportion of TH and thionin-positive pycknotic neurons with retracted cytoplasm and condensed nuclei, characteristic of apoptosis (Fig. 7A). While no pycknotic neurons were observed in SNpc of saline-injected control mice (data not shown), wild-type and CYPD knockout mice showed apoptotic cells in SNpc (Fig. 7A). Consistent with the presence of apoptotic cells in substantia nigra, morphometric analysis of fractin-immunoreactive TH-positive neurons (Fig. 7B) on day 1 and 2 following the subacute MPTP paradigm showed significant increases in fractin and TH-positive neurons in SNpc (Fig. 7C). The increase in fractin-positive neurons was significantly higher on day 1, and showed almost 2-fold increase on day 2 following MPTP. However, no significant differences were found at the level of fractin-positive cell counts between wild-type and CYPD knockout mice (Fig. 7C). These data suggest that deficiency of CYPD in mice does not alter features of apoptosis observed in the subacute paradigm of MPTP neurotoxicity, which is consistent with the lack of attenuation of dopaminergic neurotoxicity observed in this paradigm (Fig. 3).

Furthermore, the chronic continuous infusion of MPTP using mini osmotic pumps in mice causes accumulation of alpha-synuclein in nigral dopaminergic neurons (54). Although we failed to observe Lewy-body-like alpha-synuclein-immunoreactive inclusions in nigral dopaminergic neurons following the chronic infusion of MPTP, we did observe accumulation of alpha-synuclein in dopaminergic neurons following MPTP in both wild-type and CYPD knockout mice (Fig. 7D). Lack of CYPD did not impact on the quantitative accumulation of alpha-synuclein in SNpc compared to wild-type mice (Fig. 7E), suggesting that accumulation of alpha-synuclein in a chronic MPTP pump infusion model is independent of the presence or absence of CYPD. These data are consistent with the lack of neuroprotective effects observed in CYPD knockout mice against MPTP neurotoxicity in the chronic paradigm.

Discussion

The potential pathophysiological importance of PTP is well recognized, however the direct proof of its activation *in vivo* and its mode of operation is still lacking. It is well established

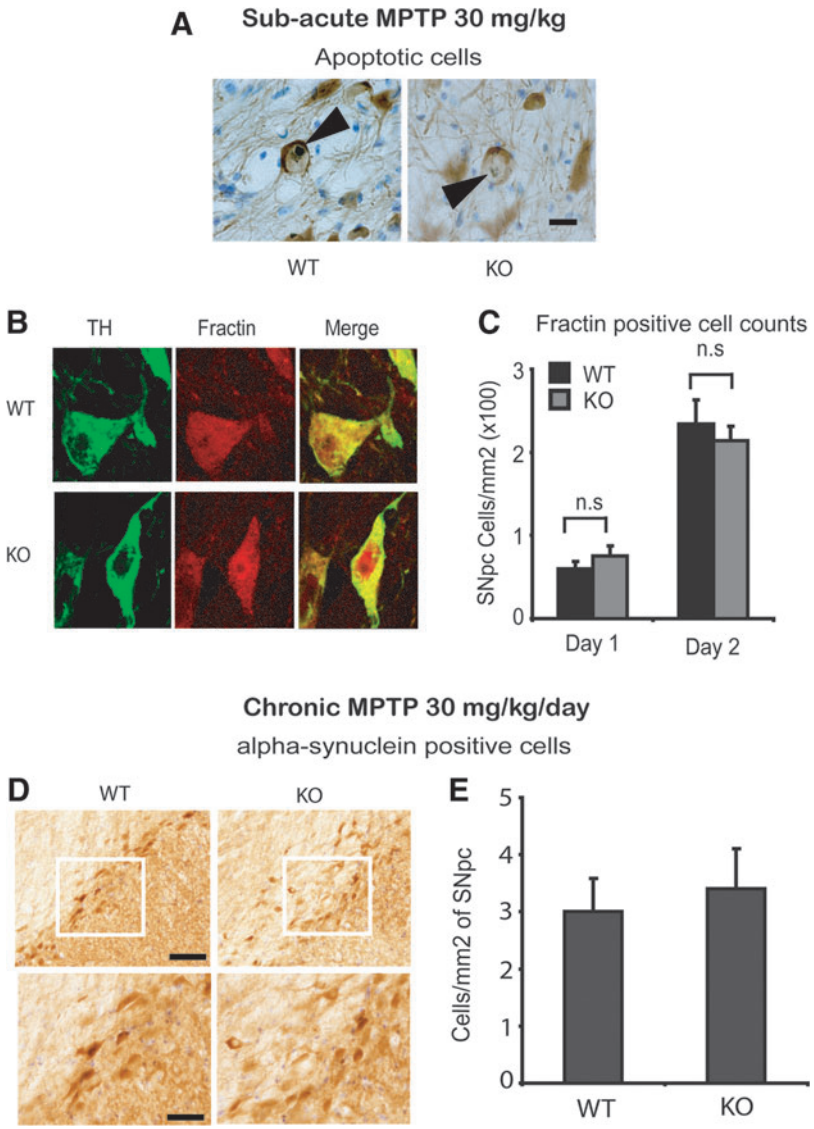

FIG. 7. CYPD knockout mice are not resistant to MPTP-induced apoptotic cell death in subacute paradigm and alpha-synuclein accumulation in chronic paradigm. (A) TH-positive apoptotic neurons in SNpc of WT and KO mice 2 days after last MPTP-injection following the subacute paradigm, representative image from 4 mice per group, Scale bar, 10 μm . **(B)** Fractin and TH-positive neurons in SNpc of WT and KO mice 2 days after last MPTP injection following the subacute paradigm, representative image from 5 mice per group, **(C)** Fractin-positive cell counts in WT and KO SNpc after 1 and 2 days following last injection of MPTP in subacute paradigm. Data represent mean ± S.E.M, $n = 5$ mice per group, n.s not significant. **(D)** alpha-Synuclein accumulation in WT and KO SNpc 1 day after chronic 28 day MPTP neurotoxicity paradigm, Scale bar, 200 μm. **(E)** alpha-Synuclein-positive cell counts in WT and KO SNpc 1 day after chronic 28 day MPTP neurotoxicity paradigm. Data represent mean ± S.E.M., $n = 5$ mice per group, n.s not significant. (To see this illustration in color the reader is referred to the web version of this article at www.liebertonline.com/ars).

that *in vitro*, PTP can be activated by Ca^{2+} overload combined with oxidative stress, de-energizing of mitochondria, and some other factors (8, 59). The ubiquitously expressed mitochondrial matrix protein CYPD is involved in the modulation of Ca^{2+} threshold for PTP open/closed probability (51). To date, the strongest indirect evidence that mitochondrial PTP is involved in modulating the outcome of tissue insult and pathology *in vivo* comes from studies with mice in which CYPD was genetically ablated. For instance, CYPD knockout mice score much better than their wild-type littermates in a mouse model of Alzheimer's disease (19) and especially in acute tissue damage paradigms such as stroke or toxic insult (4, 6, 35, 44). However, even though these studies provide strong support to the role of PTP in tissue damage, the results should be interpreted with caution. It was recently shown that in heart, CYPD ablation significantly (>25%) changes the expression of 362 genes, causes a significant increase in the glucose to palmitate ratio, suggesting a metabolic shift toward glycolysis enhances the TCA cycle flux and stimulates some metabolic mitochondrial Ca^{2+}-regulated enzymes (21). Considering that the pattern of metabolic and gene subsets involved in determining the fate of cells are different in different tissues and different disease paradigms, the contribution of CYPD in modulating the pathological outcome is expected to vary. Therefore, it has to be studied in the context of a specific disease model and injury paradigm.

A pathological activation of PTP as a consequence of elevated levels of mitochondrial Ca^{2+} has been implicated in the selective vulnerability of nigrostriatal dopaminergic neurons, suggesting that elevating the Ca^{2+} threshold for the PTP opening could block neurodegeneration. A new concept of increased vulnerability of SNpc DA neurons was recently advanced by Surmeier and colleagues (49). They note that typically SNpc DA neurons should have high proteostatic burden due to their very large axonal field with enormous number of synapses on each axon. The need to supply these axons with mitochondria should create a high metabolic load and may deplete mitochondria in the soma of these neurons. An inherent autonomous pace making activity of SNpc DA neurons results in substantial calcium fluxes through their plasma membrane and poses a burden on Ca2+-sequestering organelles. In turn, this may result in the irreversible opening of mitochondrial permeability transition and release of pro-apoptotic proteins. On the other hand, reversible opening of

PTP should not be deleterious and even be useful as it is expected to decrease ROS production and help mitochondria to re-establish their Ca2+ homeostasis, although, as the authors note, it is not known whether such reversible PTP opening is possible under the conditions of oxidative stress. The authors suggest that the chronic mitochondrial stress created by sustained Ca2+ entry could result in elevated ROS production and contribute to their selective vulnerability (49).

Here we explored the role of PTP modulator cyclophilin D in MPTP neurotoxicity. Our *in vitro* data with isolated brain mitochondria demonstrate that CYPD ablation attenuates the damage to mitochondria induced by Ca^{2+} overload. CYPD ablation clearly preserved steady-state membrane potential upon progressive Ca^{2+} loading, even in the presence of MPP^+; the CYPD knockout mitochondria exhibited higher Ca^{2+} accumulating capacity and Ca^{2+} threshold to Ca^{2+}-induced ROS production. Analysis of mitochondrial functions in ventral midbrain of CYPD knockout mice treated acutely with MPTP exhibited significantly higher activity of respiratory chain Complex I, higher rate of phosphorylating respiration, and better respiratory control index (RCI, Fig. 2A) compared to wild-type mice. These data suggest that CYPD ablation prevented MPTP-induced structural damage to inner mitochondrial membrane. However, an important aspect to consider here is that our mitochondrial functional parameters in ventral midbrain reflect the average response of mitochondria from all neurons and not specifically from substantia nigra pars compacta dopaminergic neurons that constitutes less than 5% of total neurons in ventral midbrain. Nevertheless, despite these beneficial effects of CYPD ablation on mitochondrial functions both *in vitro* and *in vivo*, nigrostriatal dopaminergic neurotoxicity were attenuated following an acute insult of MPTP intoxication and not in the subacute and chronic paradigms of MPTP.

The lack of neuroprotective effect in subacute and chronic MPTP neurotoxicity paradigms due to CYPD ablation might seem puzzling, given that our studies suggest that CYPD deficiency leads to improved mitochondrial bioenergetics functions upon MPTP intoxication. Apparently, the paradigm of MPTP delivery strongly affects the mechanism(s) of neuronal death. Important differences between acute and subacute and/or chronic MPTP mouse models extend beyond just the amount of striatal loss of dopamine and metabolites and nigral neuronal loss achieved. While both acute and subacute MPTP paradigms seemingly rely on same initial mechanisms of neurotoxicity, the mode of cell death produced in each case may be fundamentally different. Following acute administration of MPTP, nigrostriatal dopaminergic neurons appears to die primarily via nonapoptotic mechanisms involving necrosis (27, 41), whereas in the subacute paradigm nigral neurons die predominantly by apoptotic mechanisms (52). Although the exact reasons to these differences are unclear, it is suggested that differences due to frequency of dosing leading to varying response to extent of oxidative damage and microglial activation in initiating and/or perpetuating DA cell death in these two MPTP neurotoxicity paradigms are different. For instance, there is a greater degree of oxidative stress and microglial activation observed in acute than the subacute MPTP paradigm (18, 24, 31). Unlike the subacute MPTP paradigm, a more robust microglial activation observed in the acute MPTP paradigm, possibly due to a markedly increased mitochondrial complex I inhibition is known to secrete a complex array of cytokines, chemokines, and reactive oxygen/nitrogen species to create profound oxidative stress leading to a necrotic cell death in SNpc (33, 41, 55). Although we did not observe any conceivable differences in glial activation of wild-type and CYPD knockout mice following acute MPTP paradigm (Fig.6), the differences at the level of DA toxicity between the genotypes could be due to a role of CYPD in preventing acute mitochondrial bioenergetic functions, possibly induced by profound oxidative stress, microglial activation, and ATP depletion in this paradigm. Several lines of evidence indicate that mitochondrial permeability transition lead to release of pro-apoptotic proteins such as cytochrome c, whose translocation to cytosol is a critical event in the mitochondria-dependent activation of effector caspases such as caspse-3 and ensuing cell death (9). Our analysis of MPTP-induced mitochondrial cytochrome c release (Fig. 2) and assessment of apoptotic markers (data not shown) found no differences between wild-type and CYPD knockout mice (Fig. 2), and further *in vivo* analysis of apoptotic cell death in nigrostriatal dopaminergic neurons in the subacute MPTP paradigm using a caspase 3 cleaved product of actin filaments found no differences between wild-type and CYPD knockout mice (Fig. 7). Moreover, it has been demonstrated that both MPP^+-induced complex I inhibition associated and/or Bax mediated cytochrome c release is independent of mitochondrial permeability transition pore (37). These data, together with our findings from the present study, suggest that CYPD ablation plays a very little role in apoptotic cell death and provides a strong basis to the differences in neuroprotective phenotypes observed in acute and subacute/chronic MPTP paradigms in CYPD knockout mice. Although the present study provides novel mechanistic insights on the role of PTP in modulating the death of dopaminergic neurons to various paradigms of MPTP neurotoxicity, our findings not necessarily reflect a real scenario prevalent in chronic neurodegenerative disorders such as PD. Despite the ability to recapitulate selective dopaminergic cell loss, a major limiting factor in the MPTP/MPP^+ models of PD is the acute nature of insult, inability to retain striatal catecholamine loss for longer periods, poor behavioral readouts, and lack of prominent pathological signatures such as formation of protein aggregates or Lewy bodies as seen in human PD. Therefore, our results here should be interpreted by taking these factors into consideration and suggest that maybe a more realistic approach would be to test and determine the function of PTP in more progressive and chronic models of PD, especially those harboring familial PD genes (17). In this regard, elucidation of the role of PTP in other models of chronic neurodegenerative disorders such as Alzheimer's (19, 20), Huntington's disease (10), and amyotrophic lateral sclerosis (15, 34) (where mitochondrial dysfunction play a major role in disease pathogenesis) suggest that activation of PTP serves as a major arbiter of cell death in these disease models. However, it remains to be established if indeed blockers of PTP may serve as an effective therapeutic strategy for such chronic neurodegenerative disorders, including PD.

Thus, we have demonstrated that CYPD ablation is protective in an acute paradigm of MPTP poisoning, whereas it appear to be without effect upon more extended treatment with this mitochondrial toxin. It is conceivable that the primary factor responsible for the neural cell death in acute MPTP toxicity is bioenergetic failure. The product of MPTP biotransformation, MPP^+ is a strong inhibitor of mitochondrial respiratory chain Complex I, which is crucial for energy

production. MPP^+ is also capable of intense ROS production mediated by redox cycling of this compound on mitochondrial TCA enzyme α-ketoglutarate dehydrogenase complex (2, 29), which causes mitochondria-dependent oxidative stress. The latter is further augmented by the impaired mitochondrial Ca^{2+} accumulation (Fig. 1) and further increase in ROS production, most likely due to PTP opening. The emission of ROS by mitochondria that underwent PTP opening increases dramatically due to partial inhibition of their respiratory chain that is caused by the structural disruption to inner membrane and also due to the annihilation of their GSH-based H_2O_2 scavenging system as GSH and NADPH leak out of mitochondria and their concentration inside the matrix becomes insufficient for the normal functioning of mitochondrial ROS scavenging system. The ROS emission increases up to the point of full ROS-producing capacity of the respiratory chain and other mitochondrial energy-dependent ROS producing sites. This chain of events and supporting evidence had been thoroughly discussed in (1, 3, 56).

Note that *in vitro*, the MPP^+-treated CYPD knockout mitochondria initially exhibit lower ROS production and less impaired structure, less depolarization upon Ca^{2+} accumulation, and better Ca^{2+} handling (Figs. 1A–1C). This advantage disappears upon increasing the amount of Ca^{2+} added to the incubation medium. In other words, CYPD knockout mitochondria exhibit a higher Ca2+ threshold toward PTP opening, both in the absence and in the presence of MPP^+. We think these observations provide clues to why CYPD knockout mitochondria appear to be much more resistant to the effects of acute MPTP treatment *in vivo* (Fig. 2). We think that MPTP acts by (after its conversion to MPP^+) lowering the membrane potential of mitochondria. The latter is a well-known regulator of the Ca^{2+} threshold of PTP. The mechanism of CYPD effect on Ca^{2+} threshold of PTP opening is not yet known. Apparently, MPP^+ does not affect this mechanism and because of that, it similarly decreases the Ca^{2+} threshold in wild-type as well as in CYPD knockout mitochondria. However, CYPD knockout mitochondria have intrinsically higher Ca^{2+} threshold for PTP opening, which in our opinion, explains their higher resistance to MPP^+ in our experiments.

The molecular composition of PTP and the mechanism of protection achieved by CYPD ablation remain to be elucidated. However, the available information on the mechanism of CYPD-mediated PTP regulation supports the hypothesis that CYPD ablation should be protective only under conditions of acute bioenergetic failure. It was shown that CYPD inactivation or ablation modulates PTP open/closed probability by unmasking a binding site for phosphate (Pi) in the mitochondrial matrix, which inhibits PTP (7). It was also shown that CYPD binds to the stalk of the F_0F_1-ATP synthase and the binding also is modulated by Pi (25). Inactivation of CYPD caused its removal from F_0F_1-ATP synthase, which in turn stimulated the rate of ATP synthesis and hydrolysis by the enzyme; the same effect was caused by CYPD ablation (25). More recently, we demonstrated that in intact mitochondria, inhibition of CYPD by cyclosporine A or its genetic ablation stimulates the intra-mitochondrial ATP hydrolysis by the F_0F_1-ATP synthase but does not change ATP efflux or influx rates which are mediated by the adenine nucleotide translocator. This means that mitochondria where CYPD is absent or inhibited can hydrolyze ATP faster in their matrix, whereas CYPD absence would not affect their ability to supply ATP to the needs of the cell. ATP hydrolysis by F_0F_1-ATP synthase is another mechanism to energize mitochondria and maintain their membrane potential (11, 25). Maintaining the membrane potential is required for numerous mitochondrial activities, including the accumulation of the respiratory substrates and Ca^{2+} retention. Therefore, irrespective of its role in modulating PTP, CYPD deficiency may be an advantage in acute bioenergetic failure caused by an inhibition of a primary energy generator, their respiratory chain. Taken together, our data suggest that increasing mitochondrial Ca^{2+} capacity may provide temporary advantage under conditions of acute Ca^{2+} overload. However, elevated Ca^{2+} capacity is not advantageous upon prolonged exposure to mitochondria-damaging toxin such as MPTP. This certainly should be considered when evaluating the perspectives of pharmacological intervention with PTP-inhibiting compounds against dopaminergic neurodegeneration as seen in PD.

Materials and Methods

Animals

Animal studies were conducted in strict accordance with the National Institutes of Health *Guide for Care and use of Laboratory Animals* and approved by Institutional Animal Care Committee of Weill Medical College of Cornell University. CYPD knockout mice (44) were procured from Dr. Stanley Korsmeyer's laboratory. CYPD knockout mice used in this study were N-7 (seven) generations backcrossed to C57Bl6 strain. All experiments utilized littermate cohorts of age-matched male wild-type and CYPD knockout mice generated by crossing CYPD hemizygous males and females to account for potential genetic differences.

Paradigms of MPTP neurotoxicity

Three different paradigms of MPTP treatment were used in the present study. In the first paradigm, 8-week-old male mice were administered intraperitoneally (i.p.) an acute dose of 20 mg/kg free base MPTP every 2 hours four times a day, and toxicity analyses were done at day 7. In the second paradigm, which consisted of a subacute treatment, 3-month-old male mice were treated with 30 mg/kg free base MPTP once daily for a total of 5 days and toxicity analyses performed 3 weeks after the last MPTP injection. In the third paradigm, MPTP was administered in 3-month-old male mice in a chronic fashion at a dose of 30 mg/kg free base MPTP every day for 28 days using Alzet mini osmotic pumps (Model 2004, Durect Corporation), and toxicity analyses were performed on the 29^{th} day (54). Control cohorts of mice received equivalent volumes of saline at the same frequency as the respective paradigms of MPTP used in the study. All procedures involving MPTP administration in mice were performed according to standard procedures (28, 54).

Immunohistochemistry and stereological cell counts

Age- and sex- matched CYPD knockout mice and their wild-type littermates were anesthetized with sodium pentobarbital, transcardially perfused with 0.9% saline followed by 4% paraformaldehyde in 0.1 *M* PBS, pH 7.4. Brains were dissected out, post fixed in 4% paraformaldehyde for 24 h and cryopreserved in 30% sucrose/PBS for 48 h. Snap-frozen brains were coronally sectioned at 40 μm thickness using a

cryostat. Coronal sections were collected in PBS and processed free-floating for immunohistochemistry or immunofluorescence. Sections encompassing substantia nigra and striatum were washed in PBS and endogenous peroxidase was quenched by incubation with 3% H_2O_2 in 10% methanol solution for 10 min. Sections were then washed in PBS and blocked in 10% normal goat serum (NGS) or normal rabbit serum (NRS), 0.1% Triton X-100 in PBS for 1 h at room temperature (RT). Next, sections were incubated with various antibodies: rabbit polyclonal anti-tyrosine hydroxylase (TH) (1:1000) (Novus Biologicals), rat monoclonal anti-CD11b (1:500) (Serotec), rabbit polyclonal anti-glial fibrillary acidic protein (GFAP) (1:1000) (Dako), mouse monoclonal anti-alpha synuclein (1:1000) (BD Biosciences) in 2% NGS or NRS, 0.01% Triton X-100 in PBS overnight at 4°C. Sections were incubated with appropriate biotinylated horseradish peroxidase conjugated secondary antibodies (Jackson Immunoresearch) in PBS for 1 h at RT. Fractin immunostaining on sections from substantia nigra was performed following conventional procedure (36). Briefly, sections were blocked in 0.5% bovine serum albumin (BSA)/0.1% Triton X-100/ PBS at RT for 1 h, followed by incubation with rabbit polyclonal anti-fractin (1:100) (Chemicon) for 48 h at 4°C. Later sections were incubated with biotin-conjugated protein A (1:100) (Calbiochem) in BSA/PBS for 1 h at RT, following incubation in streptavidin ABC enhancer solution (Vector Laboratories) for 1 h at RT. Fractin, TH, CD11b, GFAP, and alpha-synuclein immunostaining were visualized with the chromogen diaminobenzidine (DAB) (Sigma). After PBS washes, sections were mounted on pre-coated slides (Superfrost Plus, VWR) and air-dried. Sections immunostained for TH or fractin were further counterstained with thionin (Sigma). All sections were dehydrated in ascending series of ethanol, passed through xylene, and cover slipped with mounting media (Cytoseal). Images were acquired using a Nikon Eclipse E600 microscope equipped with a digital camera. Nissl (thionin)-stained and TH-positive neuronal counts were estimated within the nigra by Stereoinvestigator software (Microbrightfield) (54). Apoptotic thionin-stained chromatin clumps were visualized in fractin-positive cells in substantia nigra (36) and were estimated by Stereoinvestigator software (Microbrightfield) and expressed as cell numbers per mm^2. Microglial activation in substantia nigra was quantified by unbiased counts of CD11b-reactive cells exhibiting conspicuous amoeboid or activated morphology (42). Astrocytic activation in substantia nigra was quantified by unbiased counts of GFAP-reactive cells exhibiting activated morphology (58). Alpha-synuclein positive cells were estimated by Stereoinvestigator software and expressed as cell numbers per mm^2.

To assess fractin co-localization with TH, double immunofluorescence labeling was performed on 40 μm-thick free-floating coronal sections from perfusion-fixed frozen brains (described above) from wild-type and CYPD knockout mice. Sections were blocked in 10% normal donkey serum (NDS) containing 0.1% Triton X-100 in PBS for 30 min at 4°C, followed by incubation with rabbit polyclonal anti-fractin antibody (1:200) and mouse monoclonal anti-TH antibody (1:200, Immunostar) in 2% NDS containing 0.1% Triton X-100 at 4°C overnight. Sections were washed in PBS and incubated in Alexa Fluor 488-conjugated donkey anti-mouse (1:200) and Alexa Fluor 594-conjugated donkey anti-rabbit (1:200) secondary antibodies (Invitrogen) in PBS containing 10% NDS, 0.1% Triton X-100 for 1 h at RT. Sections were washed in PBS three times and mounted on precoated glass slides. Slides were cover-slipped using mounting media (Immu-Mount, Thermo Shandon). For microscopic analysis, fluorescence was visualized using a confocal microscope (TCS SP5; Leica).

HPLC analysis of catecholamines and MPP^+

Striatal levels of dopamine (DA) and its metabolites 3, 4-dihydroxyphenylacetic acid (DOPAC), and homovanillic acid (HVA) were measured after sonication and centrifugation in chilled 0.1 *M* perchloric acid (PCA, 100 μl/mg tissue) as previously described (57). Briefly, 15 μl supernatant was isocratically eluted through an 80 x 4.6 mm C18 column (ESA, Inc, Chelmsford, MA) with a mobile phase containing 0.1 *M* LiH_2PO_4, 0.85 m*M* 1-octanesulfonic acid and 10% (v/v) methanol, and detected by a 2-channel Coulochem II electrochemical detector (ESA, Inc.). Concentrations of DA, DOPAC, and HVA are expressed as ng per mg protein. The protein concentrations of tissue homogenates were measured according to BCA assay (Pierce Biotech). For MPP^+ measurement, striatal tissues or isolated brain mitochondria were sonicated and centrifuged in 0.1 *M* PCA and an aliquot of supernatant was injected onto a Brownlee aquapore x 03-224 cation exchange column (Rainin, Woburn, MA). Samples were eluted isocratically with 20 m*M* boric acid-sodium borate buffer, pH 7.75, containing 3 m*M* tetrabutylammonium hydrogen sulfate, 0.25 m*M* 1-heptanesulfonic acid, and 10% isopropanol. MPP^+ levels were detected using a fluorescence detector set at excitation 295 nm and emission 375nm (57).

Mitochondrial isolation

Mitochondria were isolated from whole brains or from ventral midbrains of age-matched wild-type and CYPD knockout mice according to a modified protocol of Sims (46) adapted by us for small tissue samples. Eight-week-old male wild-type and CYPD knockout littermate mice were administered single i.p. injection of 20 mg/kg free base MPTP or saline for control group. Animals were sacrificed and ventral midbrain was collected 4 h after MPTP or saline administration. Ventral midbrain tissue ($\sim$12 mg per mouse that constitutes less than 5% of substantia nigra pars compacta dopaminergic neurons) were individually processed by manual homogenization with 2 ml Dounce-type glass pestle-glass body homogenizer in 1 ml of homogenization buffer composed of 225 m*M* mannitol, 1 m*M* EGTA, 75 m*M* sucrose, 20 m*M* HEPES/KOH (pH 7.4), and 0.2 mg/ml fatty acid free BSA. The homogenate was centrifuged at 1100 *g* for 5 min at 4°C. The supernatant was further centrifuged at 14,000 *g* for 10 min; the pellet was collected and resuspended in 0.2 ml of the homogenization medium supplemented with 12% Percoll™. The suspension was layered over 1.3 ml of the homogenization medium supplemented with 22% Percoll™ and centrifuged at 22,000 *g* for 15 min. The lower band was collected and washed twice by centrifugation at 12,000 *g* for 10 min with the homogenization buffer and once with the same buffer without EGTA and BSA. Isolated and purified mitochondria were used for the measurements within 4 h after isolation.

Mitochondrial assays

Ca^{2+} uptake in the mitochondrial suspension was measured fluorimetricaly using the mitochondria-impermeant

ratiometric dye Fura 6F as described in details (12). Mitochondrial membrane potential was measured by following the changes in fluorescence of a membrane potential-sensitive probe, safranin O, added at 20:1 (dye concentration in μM to mitochondrial protein in mg) ratio (30), with a F4500 spectrofluorimeter (Hitachi). Horseradish peroxidase and Amplex Red Ultra detection system was used to measure mitochondrial H_2O_2 emission rate. The H_2O_2 was measured from the fluorescence intensity of formed resorufin. Calibration of the H_2O_2 measuring system was performed by infusion of known amounts of H_2O_2, step-wise. Mitochondria were resuspended in 125 mM KCl, 4 mM KH_2PO_4, 14 mM NaCl, 20 mM HEPES (pH 7.2), 1 mM $MgCl_2$, 0.2 mg/ml BSA, 5 mM glutamate, 1.6 mM malate, 0.035 mM P1, P5-di (adenosine-5′-)pentaphosphate, and 0.02 mM EGTA at 37°C supplemented with 40 U/ml superoxide dismutase (30, 47, 48). Measurements of the enzyme activities in isolated mitochondria were performed according to conventional procedures as described in (22, 30, 32, 43, 45). Measurement of oxygen consumption rate in mitochondrial suspensions was measured with a Clark-type oxygen electrode and an oxymeter system connected to a computer data acquisition system ("Oxygraph", "Hansatech", UK). Mitochondria were resuspended at 0.055 mg/ml in 0.3 ml of incubation buffer composed of 125 mM KCl, 4 mM KH2PO4, 14 mM NaCl, 20 mM HEPES (pH 7.2), 1 mM $MgCl_2$, 0.2 mg/ml BSA, 5 mM glutamate, 1.6 mM malate, 0.035 mM P1,P5-di(adenosine-5′-)pentaphosphate (to suppress the activity of mitochondrial adenylate kinase for a more precise estimation of ADP:O ratio) and 0.02 mM EGTA (to compensate for the residual calcium contaminating other chemicals) at 37°C. The "resting" State 4 respiration rate was recorded for 2 min, then 200 nmols of ADP were added and the phosphorylating respiration rate (State 3) recorded for as long as it would take for mitochondria to phosphorylate added ADP and spontaneously return to the "resting" respiration (State 4a). The Respiratory Control Index (RCI) was calculated as the ratio of State 3 to State 4a rates.

Immunoblot analysis

Immunoblot analysis was performed on isolated ventral midbrain mitochondria. Mitochondria were dissolved in the TNE buffer [10 mM Tris-HCl (pH 7.4), 150 mM NaCl, 5 mM EDTA] containing protease inhibitors (5 mM PMSF, 10 μg/ml aprotinin, 10 μg/ml leupeptin, 10 μg/ml pepstatin), detergent (0.5% Nonidet P-40, 0.5% Na-deoxycholate and 1% SDS), and a phosphatase inhibitor cocktail (Sigma). The protein lysates containing equal amount of protein were separated by SDS-PAGE, electroblotted onto a nitrocellulose membrane (BioRad, Hercules, CA), and immunoreacted with an appropriate primary antibody [anti-MnSOD 1:1000 (Novus Biologicals); anti-cytochrome c 1:1000 (Abcam); anti-CYPD 1:1000 (Mitosciences), anti-Bax 1:1000 (Santa Cruz); anti-Bcl2 1:1000 (Enzo Life Sciences); anti-Bim/Bod 1:1000 (Enzo Life Sciences); anti-complex I subunit NDUFB8 1:1000 (Invitrogen), anti-Complex III Core 2 subunit UQCR2/QCR2 1:1000 (Invitrogen), anti-complex IV MT-CO1 subunit 1:1000 (Invitrogen), anti-ATPase ATP5A1 subunit 1:1000 (Invitrogen)] followed by a horseradish peroxidase-conjugated secondary antibodies (Kierkegaard Perry Labs Inc. MD). The immunoreactive proteins were visualized by incubating the blots in the chemiluminescence substrate (Pierce, Rockford, IL) and detection with ChemiDoc XRS system (Biorad). The quantitative analysis of the immunoreactive proteins was performed using NIH "ImageJ" software. Statistical analysis was performed using the ratios of the densitometric value of each band normalized to β-actin as loading control.

Statistical analysis

Results were expressed as means ± SEM. Significance was determined by one-way or two-way ANOVA, followed by the Student–Newman–Keuls test or a two-tailed unpaired Student t test. Significance was set at $p \leq 0.05$. All statistical analyses were performed using the Prism software (GraphPad, San Diego, CA).

Acknowledgments

This work was supported by National Institutes of Health Grants NS060885, NS062165 (BT), AG01493, NS065396 (AS), ES017295 (MFB), and the Michael J. Fox Foundation for Parkinson's disease (BT and MFB) and the Department of Defense (MFB).

Author Disclosure Statement

All authors declare no conflict of interest.

References

1. Adam-Vizi V and Starkov AA. Calcium and mitochondrial reactive oxygen species generation: How to read the facts. *J Alzheimers Dis* 20: S413–426, 2010.
2. Adams JD, Klaidman LK, and Cadenas E. MPP+ redox cycling: A new mechanism involving hydride transfer. *Ann NY Acad Sci* 648: 239–240, 1992.
3. Andreyev AY, Kushnareva YE, and Starkov AA. Mitochondrial metabolism of reactive oxygen species. *Biochemistry (Mosc)* 70: 200–214, 2005.
4. Baines CP, Kaiser RA, Purcell NH, Blair NS, Osinska H, Hambleton MA, Brunskill EW, Sayen MR, Gottlieb RA, Dorn GW, Robbins J, and Molkentin JD. Loss of cyclophilin D reveals a critical role for mitochondrial permeability transition in cell death. *Nature* 434: 658–662, 2005.
5. Banerjee R, Starkov AA, Beal MF, and Thomas B. Mitochondrial dysfunction in the limelight of Parkinson's disease pathogenesis. *Biochim Biophys Acta* 1792: 651–663, 2009.
6. Basso E, Fante L, Fowlkes J, Petronilli V, Forte MA, and Bernardi P. Properties of the permeability transition pore in mitochondria devoid of Cyclophilin D. *J Biol Chem* 280: 18558–18561, 2005.
7. Basso E, Petronilli V, Forte MA, and Bernardi P. Phosphate is essential for inhibition of the mitochondrial permeability transition pore by cyclosporin A and by cyclophilin D ablation. *J Biol Chem* 283: 26307–26311, 2008.
8. Bernardi P. Mitochondrial transport of cations: Channels, exchangers, and permeability transition. *Physiol Rev* 79: 1127–1155, 1999.
9. Bredesen DE, Rao RV, and Mehlen P. Cell death in the nervous system. *Nature* 443: 796–802, 2006.
10. Brustovetsky N, Brustovetsky T, Purl KJ, Capano M, Crompton M, and Dubinsky JM. Increased susceptibility of striatal mitochondria to calcium-induced permeability transition. *J Neurosci* 23: 4858–4867, 2003.
11. Chinopoulos C, Konrad C, Kiss G, Metelkin E, Torocsik B, Zhang SF, and Starkov AA. Modulation of F(0) F(1) -ATP synthase activity by cyclophilin D regulates matrix adenine nucleotide levels. *FEBS J* 278: 1112–1125, 2011.

12. Chinopoulos C, Starkov AA, and Fiskum G. Cyclosporin A-insensitive permeability transition in brain mitochondria: Inhibition by 2-aminoethoxydiphenyl borate. *J Biol Chem* 278: 27382–27389, 2003.
13. Cleren C, Starkov AA, Calingasan NY, Lorenzo BJ, Chen J, and Beal MF. Promethazine protects against 1-methyl-4-phenyl-1,2,3,6-tetrahydropyridine neurotoxicity. *Neurobiol Dis* 20: 701–708, 2005.
14. Cleren C, Yang L, Lorenzo B, Calingasan NY, Schomer A, Sireci A, Wille EJ, and Beal MF. Therapeutic effects of coenzyme Q10 (CoQ10) and reduced CoQ10 in the MPTP model of Parkinsonism. *J Neurochem* 104: 1613–1621, 2008.
15. Damiano M, Starkov AA, Petri S, Kipiani K, Kiaei M, Mattiazzi M, Flint Beal M, and Manfredi G. Neural mitochondrial Ca2+ capacity impairment precedes the onset of motor symptoms in G93A Cu/Zn-superoxide dismutase mutant mice. *J Neurochem* 96: 1349–1361, 2006.
16. Dauer W and Przedborski S. Parkinson's disease: Mechanisms and models. *Neuron* 39: 889–909, 2003.
17. Dawson TM, Ko HS, and Dawson VL. Genetic animal models of Parkinson's disease. *Neuron* 66: 646–661, 2010.
18. Dehmer T, Lindenau J, Haid S, Dichgans J, and Schulz JB. Deficiency of inducible nitric oxide synthase protects against MPTP toxicity *in vivo*. *J Neurochem* 74: 2213–2216, 2000.
19. Du H, Guo L, Fang F, Chen D, Sosunov AA, McKhann GM, Yan Y, Wang C, Zhang H, Molkentin JD, Gunn-Moore FJ, Vonsattel JP, Arancio O, Chen JX, and Yan SD. Cyclophilin D deficiency attenuates mitochondrial and neuronal perturbation and ameliorates learning and memory in Alzheimer's disease. *Nat Med* 14: 1097–1105, 2008.
20. Du H, Guo L, Zhang W, Rydzewska M, and Yan S. Cyclophilin D deficiency improves mitochondrial function and learning/memory in aging Alzheimer disease mouse model. *Neurobiol Aging* 32: 398–406, 2011.
21. Elrod JW, Wong R, Mishra S, Vagnozzi RJ, Sakthievel B, Goonasekera SA, Karch J, Gabel S, Farber J, Force T, Brown JH, Murphy E, and Molkentin JD. Cyclophilin D controls mitochondrial pore-dependent Ca(2+) exchange, metabolic flexibility, and propensity for heart failure in mice. *J Clin Invest* 120: 3680–3687, 2010.
22. Endo S, Ishiguro S, and Tamai M. Possible mechanism for the decrease of mitochondrial aspartate aminotransferase activity in ischemic and hypoxic rat retinas. *Biochim Biophys Acta* 1450: 385–396, 1999.
23. Fornai F, Schluter OM, Lenzi P, Gesi M, Ruffoli R, Ferrucci M, Lazzeri G, Busceti CL, Pontarelli F, Battaglia G, Pellegrini A, Nicoletti F, Ruggieri S, Paparelli A, and Sudhof TC. Parkinson-like syndrome induced by continuous MPTP infusion: Convergent roles of the ubiquitin-proteasome system and alpha-synuclein. *Proc Natl Acad Sci USA* 102: 3413–3418, 2005.
24. Furuya T, Hayakawa H, Yamada M, Yoshimi K, Hisahara S, Miura M, Mizuno Y, and Mochizuki H. Caspase-11 mediates inflammatory dopaminergic cell death in the 1-methyl-4-phenyl-1,2,3,6-tetrahydropyridine mouse model of Parkinson's disease. *J Neurosci* 24: 1865–1872, 2004.
25. Giorgio V, Bisetto E, Soriano ME, Dabbeni-Sala F, Basso E, Petronilli V, Forte MA, Bernardi P, and Lippe G. Cyclophilin D modulates mitochondrial F0F1-ATP synthase by interacting with the lateral stalk of the complex. *J Biol Chem* 284: 33982–33988, 2009.
26. Huser J, Rechenmacher CE, and Blatter LA. Imaging the permeability pore transition in single mitochondria. *Biophys J* 74: 2129–2137, 1998.
27. Jackson-Lewis V, Jakowec M, Burke RE, and Przedborski S. Time course and morphology of dopaminergic neuronal death caused by the neurotoxin 1-methyl-4-phenyl-1,2,3,6-tetrahydropyridine. *Neurodegeneration* 4: 257–269, 1995.
28. Jackson-Lewis V and Przedborski S. Protocol for the MPTP mouse model of Parkinson's disease. *Nat Protoc* 2: 141–151, 2007.
29. Klaidman LK, Adams JD, Jr., Leung AC, Kim SS, and Cadenas E. Redox cycling of MPP+: Evidence for a new mechanism involving hydride transfer with xanthine oxidase, aldehyde dehydrogenase, and lipoamide dehydrogenase. *Free Radic Biol Med* 15: 169–179, 1993.
30. Klivenyi P, Starkov AA, Calingasan NY, Gardian G, Browne SE, Yang L, Bubber P, Gibson GE, Patel MS, and Beal MF. Mice deficient in dihydrolipoamide dehydrogenase show increased vulnerability to MPTP, malonate and 3-nitropropionic acid neurotoxicity. *J Neurochem* 88: 1352–1360, 2004.
31. Kurkowska-Jastrzebska I, Wronska A, Kohutnicka M, Czlonkowski A, and Czlonkowska A. The inflammatory reaction following 1-methyl-4-phenyl-1,2,3, 6-tetrahydropyridine intoxication in mouse. *Exp Neurol* 156: 50–61, 1999.
32. Leong SF, Lai JC, Lim L, and Clark JB. The activities of some energy-metabolising enzymes in nonsynaptic (free) and synaptic mitochondria derived from selected brain regions. *J Neurochem* 42: 1306–1312, 1984.
33. Liberatore GT, Jackson-Lewis V, Vukosavic S, Mandir AS, Vila M, McAuliffe WG, Dawson VL, Dawson TM, and Przedborski S. Inducible nitric oxide synthase stimulates dopaminergic neurodegeneration in the MPTP model of Parkinson disease. *Nat Med* 5: 1403–1409, 1999.
34. Martin LJ, Gertz B, Pan Y, Price AC, Molkentin JD, and Chang Q. The mitochondrial permeability transition pore in motor neurons: Involvement in the pathobiology of ALS mice. *Exp Neurol* 218: 333–346, 2009.
35. Nakagawa T, Shimizu S, Watanabe T, Yamaguchi O, Otsu K, Yamagata H, Inohara H, Kubo T, and Tsujimoto Y. Cyclophilin D-dependent mitochondrial permeability transition regulates some necrotic but not apoptotic cell death. *Nature* 434: 652–658, 2005.
36. Oo TF and Burke RE. Histochemical methods for the detection of apoptosis in the nervous system. *Curr Protoc Neurosci* Chapter 1: Unit 1 15, 2007.
37. Perier C, Bove J, Wu DC, Dehay B, Choi DK, Jackson-Lewis V, Rathke-Hartlieb S, Bouillet P, Strasser A, Schulz JB, Przedborski S, and Vila M. Two molecular pathways initiate mitochondria-dependent dopaminergic neurodegeneration in experimental Parkinson's disease. *Proc Natl Acad Sci USA* 104: 8161–8166, 2007.
38. Petronilli V, Penzo D, Scorrano L, Bernardi P, and Di Lisa F. The mitochondrial permeability transition, release of cytochrome c and cell death. Correlation with the duration of pore openings in situ. *J Biol Chem* 276: 12030–12034, 2001.
39. Przedborski S and Jackson-Lewis V. Mechanisms of MPTP toxicity. *Mov Disord* 13: 35–38, 1998.
40. Przedborski S, Tieu K, Perier C, and Vila M. MPTP as a mitochondrial neurotoxic model of Parkinson's disease. *J Bioenerg Biomembr* 36: 375–379, 2004.
41. Przedborski S and Vila M. The 1-methyl-4-phenyl-1,2,3,6-tetrahydropyridine mouse model: A tool to explore the pathogenesis of Parkinson's disease. *Ann NY Acad Sci* 991: 189–198, 2003.
42. Reynolds AD, Banerjee R, Liu J, Gendelman HE, and Mosley RL. Neuroprotective activities of CD4+CD25+ regulatory T cells in an animal model of Parkinson's disease. *J Leukoc Biol* 82: 1083–1094, 2007.

43. Rose IA and O'Connell EL. Mechanism of aconitase action. I. The hydrogen transfer reaction. *J Biol Chem* 242: 1870–1879, 1967.
44. Schinzel AC, Takeuchi O, Huang Z, Fisher JK, Zhou Z, Rubens J, Hetz C, Danial NN, Moskowitz MA, and Korsmeyer SJ. Cyclophilin D is a component of mitochondrial permeability transition and mediates neuronal cell death after focal cerebral ischemia. *Proc Natl Acad Sci USA* 102: 12005–12010, 2005.
45. Shepherd D and Garland PB. *Methods Enzymol* 13: 11–16, 1969.
46. Sims NR. Rapid isolation of metabolically active mitochondria from rat brain and subregions using Percoll density gradient centrifugation. *J Neurochem* 55: 698–707, 1990.
47. Starkov AA. Measurement of mitochondrial ROS production. *Methods Mol Biol* 648: 245–255, 2010.
48. Starkov AA, Polster BM, and Fiskum G. Regulation of hydrogen peroxide production by brain mitochondria by calcium and Bax. *J Neurochem* 83: 220–228, 2002.
49. Surmeier DJ, Guzman JN, and Sanchez-Padilla J. Calcium, cellular aging, and selective neuronal vulnerability in Parkinson's disease. *Cell Calcium* 47: 175–182, 2010.
50. Suzuki K, Mizuno Y, Yamauchi Y, Nagatsu T, and Mitsuo Y. Selective inhibition of complex I by N-methylisoquinolinium ion and N-methyl-1,2,3,4-tetrahydroisoquinoline in isolated mitochondria prepared from mouse brain. *J Neurol Sci* 109: 219–223, 1992.
51. Tanveer A, Virji S, Andreeva L, Totty NF, Hsuan JJ, Ward JM, and Crompton M. Involvement of cyclophilin D in the activation of a mitochondrial pore by Ca2+ and oxidant stress. *Eur J Biochem* 238: 166–172, 1996.
52. Tatton NA and Kish SJ. In situ detection of apoptotic nuclei in the substantia nigra compacta of 1-methyl-4-phenyl-1,2,3,6-tetrahydropyridine-treated mice using terminal deoxynucleotidyl transferase labelling and acridine orange staining. *Neuroscience* 77: 1037–1048, 1997.
53. Thomas B. Parkinson's disease: From molecular pathways in disease to therapeutic approaches. *Antioxid Redox Signal* 11: 2077–2082, 2009.
54. Thomas B, von Coelln R, Mandir AS, Trinkaus DB, Farah MH, Leong Lim K, Calingasan NY, Flint Beal M, Dawson VL, and Dawson TM. MPTP and DSP-4 susceptibility of substantia nigra and locus coeruleus catecholaminergic neurons in mice is independent of parkin activity. *Neurobiol Dis* 26: 312–322, 2007.
55. Wu DC, Jackson-Lewis V, Vila M, Tieu K, Teismann P, Vadseth C, Choi DK, Ischiropoulos H, and Przedborski S. Blockade of microglial activation is neuroprotective in the 1-methyl-4-phenyl-1,2,3,6-tetrahydropyridine mouse model of Parkinson disease. *J Neurosci* 22: 1763–1771, 2002.
56. Yamashima T. Ca2+-dependent proteases in ischemic neuronal death: A conserved 'calpain-cathepsin cascade' from nematodes to primates. *Cell Calcium* 36: 285–293, 2004.
57. Yang L, Calingasan NY, Thomas B, Chaturvedi RK, Kiaei M, Wille EJ, Liby KT, Williams C, Royce D, Risingsong R, Musiek ES, Morrow JD, Sporn M, and Beal MF. Neuroprotective effects of the triterpenoid, CDDO methyl amide, a potent inducer of Nrf2-mediated transcription. *PLoS One* 4: e5757, 2009.
58. Yin F, Banerjee R, Thomas B, Zhou P, Qian L, Jia T, Ma X, Ma Y, Iadecola C, Beal MF, Nathan C, and Ding A. Exaggerated inflammation, impaired host defense, and neuropathology in progranulin-deficient mice. *J Exp Med* 207: 117–128, 2010.
59. Zoratti M and Szabo I. The mitochondrial permeability transition. *Biochim Biophys Acta* 1241: 139–176, 1995.

Address correspondence to:
Dr. Bobby Thomas
Department of Neurology and Neuroscience
Weill Medical College of Cornell University
525 East 68th St., A-501
New York, NY 10065

E-mail: bot2003@med.cornell.edu

or

Dr. Anatoly Starkov
Department of Neurology and Neuroscience
Weill Medical College of Cornell University
525 East 68th St., A-501
New York, NY 10065

E-mail: ans2024@med.cornell.edu

Date of first submission to ARS Central, December 18, 2010; date of final revised submission, April 21, 2011; date of acceptance, April 29, 2011.

Abbreviations Used

Ca^{2+} = calcium
CYPD = cyclophilin D
DA = dopamine
DOPAC = 3,4-dihydroxyphenylacetic acid
GFAP = glial fibrillary acidic protein
H_2O_2 = hydrogen peroxide
HPLC = high performance liquid chromatography
HVA = homovanillic acid
MPP^+ = 1-methyl-4-phenyl-pyridinium ion
MPTP = 1-methyl-4-phenyl-1,2,3,6-tetrahydropyridine
NADPH = nicotinamide adenine dinucleotide phosphate-oxidase
NGS = normal goat serum
NRS = normal rabbit serum
PBS = phosphate buffered saline
PCA = perchloric acid
PD = Parkinson's disease
PTP = permeability transition pore
ROS = reactive oxygen species
SDS-PAGE = sodium dodecyl sulphate polyacrylamide gel electrophoresis
SNpc = substantia nigra pars compacta
TH = tyrosine hydroxylase
WT = wild type